Band gap stability in CeRhSb

A. Ślebarski
Institute of Physics, University of Silesia, 40-007 Katowice, Poland

A. Jezierski
Institute of Molecular Physics, Polish Academy of Sciences, 60-179 Poznań, Poland

A. Zygmunt
Institute for Low Temperature and Structure Research, Polish Academy of Sciences, 50-950 Wrocław, Poland

S. Mähl and M. Neumann
Universität Osnabrück, Fachbereich Physik, 49069 Osnabrück, Germany

(Received 9 April 1998; revised manuscript received 22 July 1998)

The electronic structure and magnetic properties of CeRhSb were investigated by substituting Rh with 10% of Pd or Co, or Sb with 10% Sn. The $3d$ and $4d$ x-ray photoelectron spectroscopy (XPS) spectra show that CeRhSb and its alloys with Pd and Co are mixed valent. For Sn, the spectra are consistent with trivalence. Analysis of the f^2 weight in the $3d$ XPS spectra using Gunnarsson-Schönhammer theory suggests a hybridization constant of 140 meV for CeRhSb and about 170 meV for its alloys. Linearized muffin-tin orbital calculations give a pseudo-V-shape gap located at the Fermi level. This classifies these materials as semimetals rather than semiconductors. The location of the pseudogap in CeRhSb varies with the number of valence electrons. We discussed the correlation between the gap at the Fermi level and the number of free electrons, the valence of Ce, and the f-d hybridization. [S0163-1829(98)00644-4]

I. INTRODUCTION

Ce-based compounds such as CeNiSn,[1,2] CeRhSb,[3] and $Ce_3Bi_4Pd_3$ (Ref. 4) belong to a class of rare-earth compounds that become semiconducting at low temperatures (Kondo insulators). However, they are not ordinary semiconductors because the gap formation is due to many-body interactions between conduction and localized electrons in the f shell. It is generally accepted that the small gaps in the range of 10–100 K in Kondo insulators originate from weak hybridization between localized f levels and the conduction band. In terms of a simple Kondo model, the gap would also correspond to the filling of the Brillouin zone by additional states due to the Abrikosov-Suhl resonance.[5] An insulating gap formation is indeed theoretically expected for Kondo systems without long-range magnetic order and with a certain Coulomb interaction U between the f states $(U \neq 0)$.[6]

Previous alloying studies show that the energy gap in Ce-based Kondo insulators is very sensitive to the partial substitution of either Ce by La or Ni (Rh) by a transition metal.[7–9] Replacing all Ce ions of the Kondo insulator by trivalent ions leads to ordinary metals, whereas by replacing the Ce ions such by tetravalent non-f ions such as Zr, Ti, or Hf, semiconductors are obtained. This predicts a ground state of the known Kondo insulators as a result of the hybridization of one occupied f state with a half-filled conduction band.

However, the problem of the ground state of CeNiSn and CeRhSb still exists. A Sn nuclear magnetic resonance study reported a semimetallic ground state with a V-shaped pseudogap and with a low carrier of the density of states (DOS) at the Fermi level.[10] Recently, we investigated the electronic structure of the alloyed CeNiSn.[11,12] The x-ray photoelectron spectroscopy (XPS) results and the self-consistent spin-polarized linear muffin-tin orbital (LMTO) calculations clearly indicated the indirect gap, which is unstable against any change in $4f$ conduction electron hybridization caused by alloying. The gap was visible only in these CeNiSn alloys which contain the mixed valence Ce ions, but the LMTO calculations always gave a small number of the DOS at the Fermi level.

In this work we present the electronic structure and magnetic properties of CeRhSb when Rh or Sb is respectively replaced by 10% of Co and Pd or Sn. The major attention concerns the comparison of the valence-band XPS spectra with calculations of the electronic structure of the valence bands. The pseudo-V-shape gap was always calculated for the investigated CeRhSb-type alloys, however, its energetic location in the bands near ϵ_F is dependent on the respective substituted element. It is also found that the substitution of Co, Pd, or Sn modifies the V-shaped pseudogap in CeRhSb and generates the DOS plateau over a very small energy range near ϵ_F. We also note the correlation between the mixed valence of Ce ions and the gap formation at the Fermi level in the alloyed CeRhSb. We will also present the $3d$ and $4d$ core-level XPS Ce spectra and discuss their implications for the structure of the $4f$ levels in the conduction bands. We will show that f-level hybridization with the conduction band is important in CeRhSb alloys.

II. EXPERIMENT

The samples CeRhSb, $CeRh_{0.9}Co_{0.1}Sb$, $CeRh_{0.9}Pd_{0.1}Sb$, and $CeRhSb_{0.9}Sn_{0.1}$ were arc melted on a cooled copper crucible in a high-purity argon atmosphere, remelted ten times, and then annealed at 800 °C for one week. The constituents were specpure.

The x-ray analysis showed single phase samples within the usual resolution of 6%, which crystallized in the orthorhombic TiNiSn-type structure (space group *Pnma*).

A SQUID magnetometer and vibrating magnetometer were used to obtain the magnetization results for low temperatures from 1.6 K up to 300 K and magnetic fields of 50 Oe to 50 kOe.

The XPS spectra were obtained with monochromatized Al $K\alpha$ radiation at room temperature using a PHI 5600ci ESCA spectrometer. The spectra were measured immediately after cleaving the sample in vacuum below 6×10^{-10} Torr. Calibration of the spectra was performed according to Ref. 13. Binding energies were referenced to the Fermi level ($\epsilon_F=0$), the $4f$ levels of gold were found at 84.0 eV, and the observed energy spread of electrons detected at the Fermi energy was about 0.4 eV. In all investigated Ce alloys we have detected in the XPS spectra a very small amount of oxygen, which mainly arises from the impurity phase Ce_2O_3.

The electronic structure of the ordered CeRhSb alloys was studied by the self-consistent tight-binding linearized muffin-tin orbital method[14] within the atomic sphere approximation (ASA) and the local spin density (LSD) approximation. The exchange correlation potential was assumed in the form proposed by von Barth-Hedin[15] and Langreth-Mehl-Hu (LMH)[16] with corrections included. In the band calculations we assumed the initial configurations according to the Periodic Table of elements. The electronic structures were computed for the experimental lattice parameters for the supercell $Ce_8Rh_7MSn_8$ or $Ce_8Rh_8Sb_7M$, where M is Co, Pd, or Sn for 144 k points in the irreducible part of the Brillouin zone. The value of the Wigner-Seitz radii in the atomic sphere approximation was chosen to satisfy the conditions $\Sigma_n(S_n/S)^3=N$, where $S=a(3/4\pi N)^{1/3}$. Here a denotes the lattice parameter, N is the number of atoms in the cell, and the summation was made for all atoms in the cell.

III. RESULTS AND DISCUSSION

A. Magnetic properties

The magnetic susceptibility of CeRhSb shown in Fig. 1 was discussed recently in Ref. 3. It is typical for a cerium valence-fluctuation compound; the susceptibility exhibits a broad maximum at about 120 K and at higher temperatures it follows a Curie-Weiss behavior with an effective moment ($\mu_{\rm eff}$) which is close to the free ion value with $J=5/2$ and a Weiss constant $\Theta=-290$ K (Fig. 1). The large value of Θ arises from strong crystal-field effects (three doublets relatively far-lying), a Kondo interaction, or from both. Below 50 K, CeRhSb shows a susceptibility which corresponds to about 2% of trivalent Ce due to incomplete solution of Ce in the alloy.[3] The incomplete solution of Ce in cerium valence-fluctuation compounds is often observed, since no secondary phases are detected in the sample within the x-ray limit (e.g., Ref. 17).

The ionic two-level interconfiguration fluctuation (ICF) model proposed by Sales and Wohlleben[18] can determine how much of the susceptibility reported in Fig. 1 is intrinsic. Sales and Wohlleben used the formula $\chi(T)=N\mu^2n_f(T)/3k_B(T+T_f)$, where the valence fraction $n_f(T)$ is computed based on a Boltzmann statistic for an ionic two-level system ($4f^1$, $4f^0$). The trivalent magnetic level is higher than the nonmagnetic one by an energy E_x of order $2T_{\rm max}$.[19] T_{sf}, which is essentially equal to Θ, is interpreted in this model as the inverse of the valence fluctuation lifetime. The solid lines in Fig. 1 represent the $\chi(T)=\chi_0+nC/T+N\mu^2n_f^\chi/3k_B(T+T_{sf})$ [and $\chi^{-1}(T)$] fits based on the ICF model with parameters given in Table I. A Curie-Weiss term nC/T explains the observed upturn in susceptibility caused by a fraction n of paramagnetic Ce impurities. The $T=1.5$ K susceptibility increment $\Delta\chi\cong C/2\Theta$ either for CeRhSb or for the doped samples, since the upturn in susceptibility caused by a fraction of n paramagnetic impurities Ce^{3+} has been subtracted, i.e., the scaling behavior $\Theta:T_{\rm max}:C/\chi(0)$ for the valence fluctuating systems occurs.

The $(\chi T)^{1/2}$ plot in Fig. 1 tells us that $\mu_{\rm eff}$ of CeRhSb is about $2.1\mu_B$ at 300 K, which is less than the Hund's rule value of the free ion Ce^{3+}. At 1.5 K, free carriers do not compensate the local magnetic moment due to the local Kondo interaction. The remanence $\mu_{\rm eff}=0.3\mu_B$ is mainly

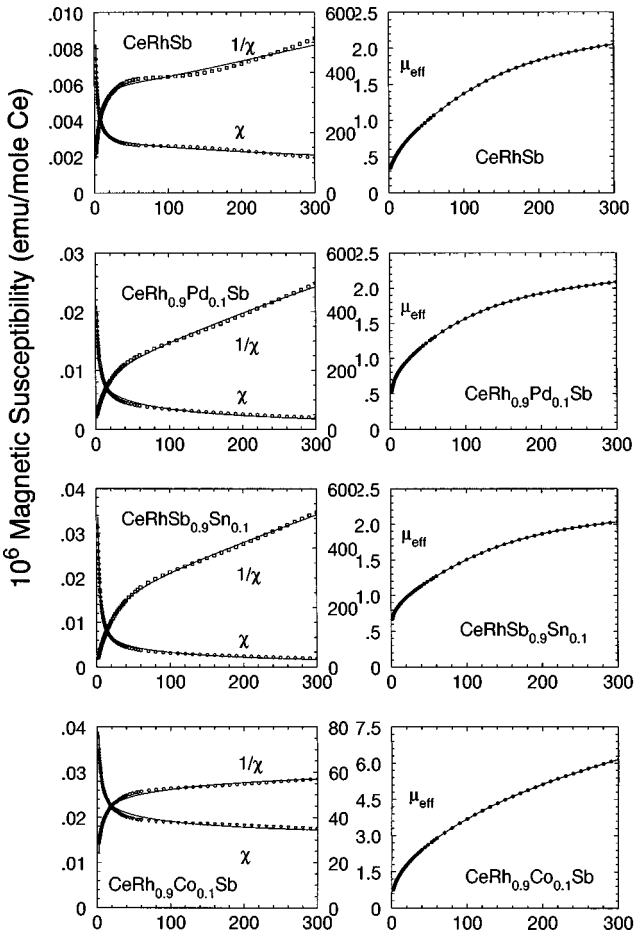

FIG. 1. Magnetic susceptibility χ in emu/(mol formula unit) and inverse susceptibility χ^{-1} in $(\text{cm}^3/\text{mol formula unit})^{-1}$. The applied magnetic field is 10 kOe. The solid line is a fit based on the ICF model with parameters given in Table I. The plots on the right side present the effective magnetic moment $\mu_{\rm eff}$ per one Ce atom in μ_B as a function of temperature [the effective magnetic moment at each T is $(\chi T)^{1/2}(3k_B/N)^{1/2}$, where k_B is the Boltzmann constant and N is the Avogadro number]. Hund's rule $\mu_{\rm eff}$ of the free Ce^{3+} is $2.54\mu_B$.

TABLE I. The crystallographic and magnetic properties and the results of TB LMTO band-structure calculations. The values of χ_0, n, T_{sf}, and E_x/k_B are defined by fitting $\chi(T)$ to the experimental magnetic susceptibility data. Curie-Weiss temperature θ is obtained from the linear relation of χ^{-1} vs T. n_f^{χ} is an occupation number obtained from susceptibility. Δ is the hybridization constant. The calculations were carried out for the $Ce_8Rh_7MSb_8$ (M=Co or Pd) and $Ce_8Rh_8Sb_7Sn$ supercells. ϵ_g is the energy of the minimum of the pseudo-V-shape gap with respect to the Fermi level ϵ_F.

	CeRhSb	$CeRh_{0.9}Co_{0.1}Sb$	$CeRh_{0.9}Pd_{0.1}Sb$	$CeRhSb_{0.9}Sn_{0.1}$
lattice parameters a, b, c in Å	4.6124	4.6076	4.6301	4.6217
	7.4130	7.4322	7.4424	7.4151
	7.8531	7.8338	7.8775	7.8639
χ_0 in emu/mol	7.4×10^{-4}	1.6×10^{-2}	4.1×10^{-4}	3.1×10^{-4}
impurity concentration n	0.016	0.051	0.053	0.093
Θ in K	290		160	180
T_{sf} in K	250	143	124	132
E_x in K	412	0	194	316
n_f^{χ} at T=300 K	0.71	0.86	0.79	0.74
$n_f^{\mathrm{XPS}}=1-\frac{I(f^0)}{I(f^0)+I(f^1)+I(f^2)}$	0.86	0.89	0.86	<1
Δ in meV	140	170	150	160
ϵ_g in eV	-0.030	-0.025	-0.074	$+0.023$
DOS at ϵ_g in states/eV at	0.27	0.32	0.22	0.44
DOS at ϵ_F in states/eV at	0.37	0.37	1.07	0.82

due to paramagnetic Ce^{3+} impurities and an incomplete correction of χ, as the susceptibility of the lanthanum analog sample was not subtracted.

The susceptibilities of the samples with 10% Pd or Sn are comparable to that of CeRhSb at high temperatures (Fig. 1). Also the $(\chi T)^{1/2}$ plots in Fig. 1 show almost the same values of about $2.1\mu_B$. At low temperature, however, susceptibilities of the Pd and Sn samples are higher than for CeRhSb. The ratio $\mu_{\mathrm{eff}}(\mathrm{alloy})/\mu_{\mathrm{eff}}(\mathrm{CeRhSb})$ at T=1.5 K is 1.7 and 2.1 for the Pd and the Sn sample, respectively. Moreover, the Weiss Θ constant is strongly reduced to -160 K for the Pd and -180 K for the Sn alloys. An increase in the low-temperature susceptibility and the decrease in Curie-Weiss Θ suggest that the Kondo temperature decreases by about 30% for Sn and Pd doping. The ICF model explains well the susceptibilities of the Pd- and Sn-doped samples and gives almost the same ratio $T_{sf}/\Theta\cong0.8$ (Table I). In addition, the magnetization σ of CeRhSb and its Pd and Sn alloys is linear with the magnetic field H (Fig. 2) and the slope of $\sigma(H)$ increases in the alloys. One can discuss the increment of $\sigma(H)$ in terms of an incomplete solution of Ce atoms in the alloy in agreement with an analysis of a Curie-Weiss term of the susceptibility (Table I). The electronic configurations of Rh and Pd and of Sb and Sn are similar and the concentration and the atomic position of Ce is unchanged in all investigated samples. The number of the d electrons is slightly increased in the Pd alloy. We also note the shift of the broad maximum in χ to a lower temperature. This suggests the lowering of the mixed valence of Ce ions in the Pd alloy, which we can attribute to the occupation number of the $4d$ subband. In this picture, very similar behavior of $\sigma(H)$ and $\chi(T)$ of the Sn alloy seems to be surprising. Partial substitution of Sb by Sn lowers the number of $5p$ electrons. Thus, the p subband, located below ϵ_F, could be occupied by conduction electrons of Ce or Rh atoms due to intra-atomic hybridization. This also can lead to a smaller occupation number of the $4f$ shell and simultaneously to a larger mixed valence of Ce ions. Second, the lower number of Rh $4d$ electrons should also increase the valence of Ce. However, the $\chi(T)$ plot in Fig. 1 does not show any maximum, which would be characteristic in a valence fluctuation. Instead of this, we expect a change of the gap in CeRhSb as a result of the changed number of occupied states in the $5p$ subband which is located close to ϵ_F. Actually, the width of the gap is reduced, as will be described later.

At helium temperature the susceptibility of the Co alloy is nearly the same as for the Pd or Sn alloy, however between 50 K and 300 K it is 10 times larger and almost temperature independent (Fig. 1). Also the $\sigma(H)$ dependence shown in Fig. 2 is quite different from the other alloys and suggests some additional influence of Co. At 300 K, a huge magnetic moment $(\chi T)^{1/2}$ of about $6\mu_B$ is observed, which suggests a spin-glass system with Co clusters. Also a percolation of Co moments in coexistence with a Kondo state cannot be fully

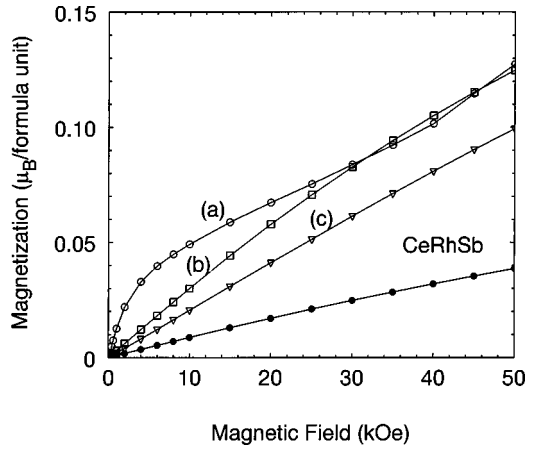

FIG. 2. Magnetization of CeRhSb, $CeRh_{0.9}Co_{0.1}Sb$ (a), $CeRhSb_{0.9}Sn_{0.1}$ (b), and $CeRh_{0.9}Co_{0.1}Sb$ (c), at T=4.2 K.

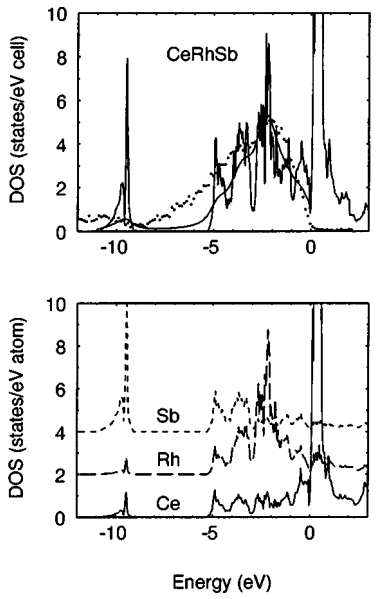

FIG. 3. Comparison of the total DOS (solid line), the convoluted DOS (by Lorentzians of the half-width 0.4 eV and taking into account proper cross sections for bands with different l symmetry; dashed line), and the measured XPS valence bands corrected by the background (points) for CeRhSb. The partial DOS are plotted below.

excluded. The susceptibility maximum—if it exists—is not observed because of the strongly enhanced paramagnetic susceptibility of the Co sublattice.

In the following, the magnetic properties of the CeRhSb and its Pd, Co, and Sn alloys will be correlated with their electronic structure, which was determined by XPS spectra and band-structure calculations.

B. Electronic structure of the alloyed CeRhSb

In Figs. 3–6, a comparison of LMTO valence-band calculations with XPS spectra is shown for the four different CeRhSb alloys. In each case, good agreement between experiment and theory can be seen. The DOS are convoluted by Lorentzians with a half-width 0.4 eV. The partial densities of states were multiplied by the corresponding cross sections, which are taken from Ref. 20. The XPS bands are subtracted by the background which was calculated by a Tougaard algorithm.[21] The broad peaks located near ϵ_F in the XPS valence-band spectra are mainly attributed to d states of Rh. The intensities of those peaks are only slightly modified when Rh in CeRhSb is replaced in part by Co or Pd. The second peak located at about 10 eV in the bands represents mainly the Sb states. The partial DOS presented in Figs. 3–6 show a renormalized f level. No significant influence of alloying was observed in the shape of the Ce subbands, however at ϵ_F the density of the Ce states is two times larger in the Sn alloy than in the other CeRhSb alloys. The calculations give also comparable occupation numbers of the Ce states in the alloys, which are about 1.30, 1.85, 0.47, and 0.66 for the $4f$, $5d$, $6s$, and $6p$ states, respectively. Likewise, the partial DOS of Rh and Sb did not distinctly depend on alloying. By changing the number of the valence electrons in CeRhSb, the shape of the bands is only slightly modified, however the position of the Fermi level is much

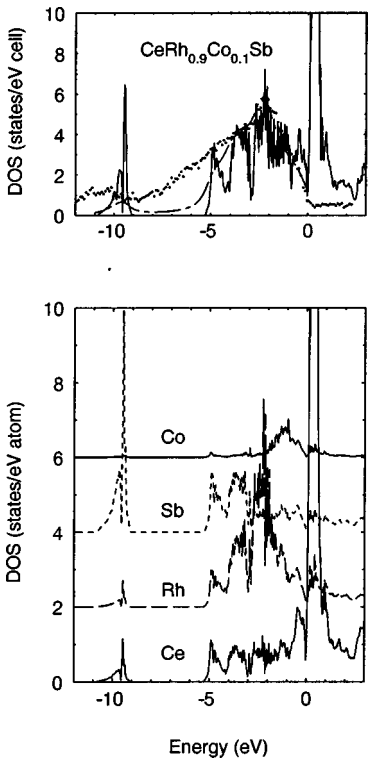

FIG. 4. Comparison of the total DOS (solid line), the convoluted DOS, and the measured XPS valence bands corrected by the background (points) for $CeRh_{0.9}Co_{0.1}Sb$. The partial DOS are plotted below.

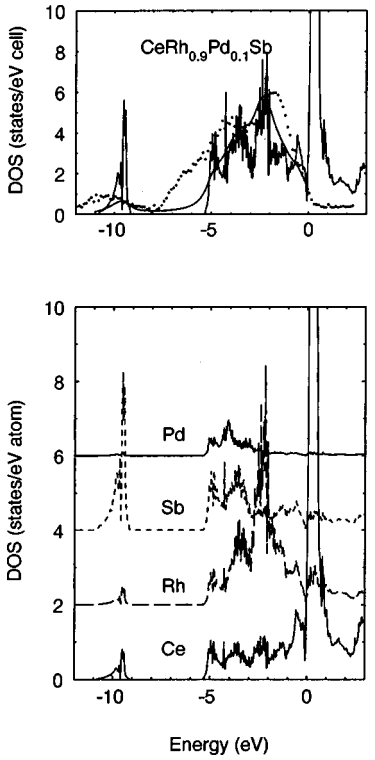

FIG. 5. Comparison of the total DOS (solid line), the convoluted DOS, and the measured XPS valence bands corrected by the background (points) for $CeRh_{0.9}Pd_{0.1}Sb$. The partial DOS are plotted below.

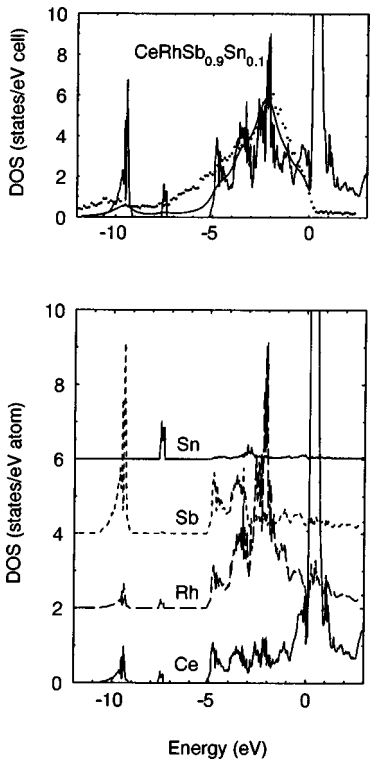

FIG. 6. Comparison of the total DOS (solid line), the convoluted DOS (partial DOS are shown below), and the measured XPS valence bands corrected by the background (points) for $CeRhSb_{0.9}Sn_{0.1}$.

more influenced. Partial substitution of Sb by Sn (the atomic radii of both elements are similar) leads to a shift of the bands to lower binding energies, which also shifts the gap energy ϵ_g (Table I). The number of valence electrons is increased when Rh is partly replaced by Pd. This substitution moves ϵ_g to higher binding energy. Substitution of Co did not lead to significant changes in ϵ_g, as the total number of valence electrons is not changed. Only changes of the local environment of each atom in the unit cell occur. The shift of ϵ_g per n additional electrons in the valence band was estimated to be $\epsilon_g/n = 0.4$ eV/electron. Increasing or decreasing the number n, the DOS at the Fermi level is always increased with respect to CeRhSb (Fig. 7).

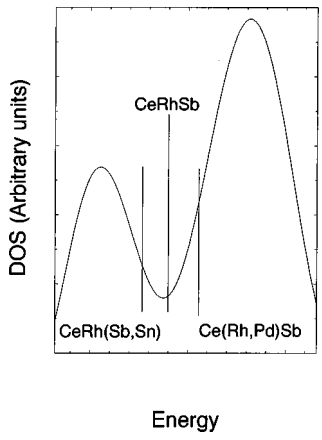

FIG. 7. Schematic DOS with the V-shaped pseudogap in relation to the Fermi level (perpendicular lines) in CeRhSb alloys.

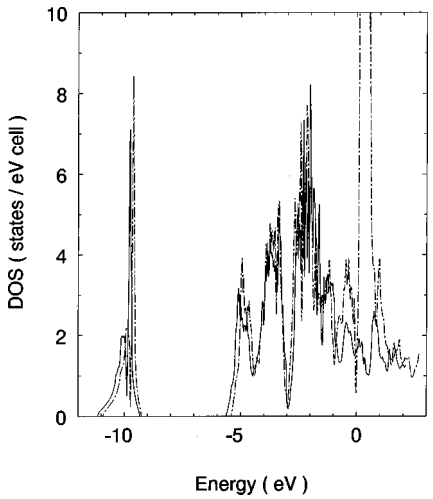

FIG. 8. The numerical results for CeRhSb with the Ce $4f$ electrons treated as band electrons (dotted line) and with the Ce $4f$ as a frozen core state (solid line).

In band-structure calculations, the Ce $4f$ electrons are treated as band electrons. In reality, they are more localized, and to treat them correctly, band theory would have to include strong local correlations. These correlations could cause the numerical changes (e.g., the shift in the gap energy and the changes in the density of states at the Fermi level and at the gap energy) in the band. One way to explore this issue would be to carry out the calculations treating the Ce $4f$ as a frozen core state, and see how the numerical results change. We applied the model of Brooks *et al.*[22] We treated the localized $4f^1$ states of Ce as core states, which do not hybridize with conduction electrons. In this way there is no $4f$ contribution to the density of states. The calculations treating the Ce $4f$ as a frozen core state have never given the gap and the density of states at the Fermi level is much larger than for the $4f$ electrons treated as band electrons (Fig. 8). We obtained the analogous numerical results for the localized Ce $4f$ electrons for Co, Pd, and Sn doping.

In conclusion, band-structure calculations on CeRhSb show that a V-shaped gap formation is strongly dependent on the *f*-conduction electrons hybridization. In our opinion, the hybridization between the Ce $4f$ states and the transition-metal–d states seems to be very important to the formation of the gap in CeRhSb (and in CeNiSn). However, local correlations can have a destructive influence on the gap. This is a competitive effect to f-d hybridization near the Fermi level, which can alter the densities of states at the gap energy and form the pseudogap.

Figure 9 presents the band structures of CeRhSb alloys plotted along various symmetry directions. The energy bands of CeRhSb alloys are similar. The indirect gap is strongly anisotropic. It is closed mainly in the Γ-X and Γ-Z directions and is the biggest at the Y point. For Co and Pd alloys, the gap is reduced in Y by about 30% with respect to CeRhSb, but for Sn the reduction is more than 60%.

X-ray photoelectron spectroscopy is not an ideal probe for the Ce $4f$ valence bands because of the relatively small cross sections. The XPS spectra of the $3d$ core levels, however, give more information about the $4f$ shell configurations and hybridization. The intensity of the $3d$ lines in the Ce inter-

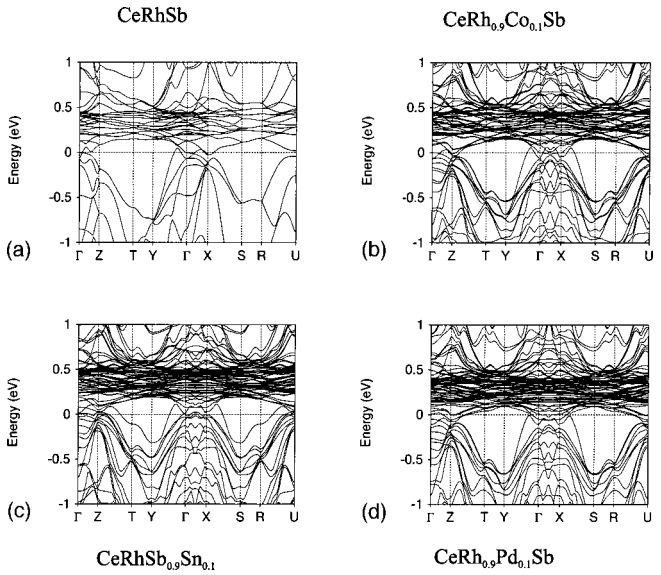

FIG. 9. TB LMTO band structure of CeRhSb (a), $CeRh_{0.9}Co_{0.1}Sb$ (b), $CeRhSb_{0.9}Sn_{0.1}$ (c), and $CeRh_{0.9}Pd_{0.1}Sb$ (d) along various symmetry directions in the Brillouin zone.

metallic compounds shows different final states depending on the occupation of the f shell.[23,24] Figure 10 represents the Ce $3d$ XPS spectra of the CeRhSb alloys. Three final-state contributions f^0, f^1, and f^2 are observed, which exhibit a spin-orbit splitting $\Delta_{SO}=18.3$ eV. The appearance of the f^0 components is clear evidence of the mixed valence. For $CeRhSb_{0.9}Sn_{0.1}$, no clear f^0 components are observed, which predicts a stable $4f$ configuration of Ce. Based on the Gunnarsson-Schönhammer theoretical model,[23,24] the intensity ratio $I(f^0)/I(f^0)+I(f^1)+I(f^2)$, which should be directly related to the f-occupation probability in the final states, indicates an f-occupation number n_f^{XPS} (Table I). To compare the experimental results from the XPS spectroscopy and from the susceptibility, we note that each type of experiment yields a different picture of the electronic states in α-Ce in CeRhSb and in the doped alloys. For CeRhSb and the Co- and Pd-doped samples, XPS indicates an f-occupation number about twice as large as n_f obtained from the susceptibility. These discrepancies show immediately

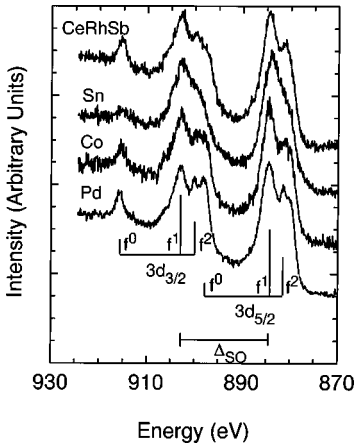

FIG. 10. Ce $3d$ XPS spectra obtained for several CeRhSb alloys. The $3d^9 4f^1$, $3d^9 4f^0$, and $3d^9 4f^2$ components are separated on the basis of the Doniach-Šunjić theory.

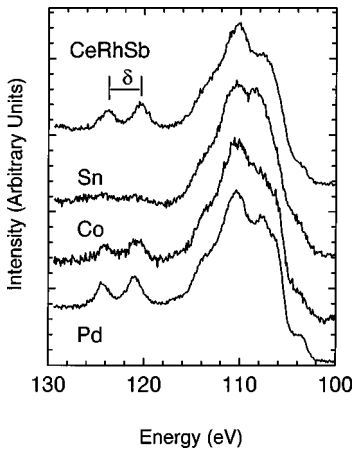

FIG. 11. XPS spectra of the 4d core levels of CeRhSb alloys.

that the final-state f occupation is smaller for a ''fast'' (XPS) experiment than for a ''slow'' one (susceptibility). However, the largest divergence of n_f in the Sn-doped alloy is not clear.

In Fig. 11, the Ce $4d$ XPS spectra are shown. Again, clear evidence for mixed valence in CeRhSb and the Co and Pd alloys is seen, although no detailed interpretation of the spectra is attempted because of the strong multiplet splittings. The two peaks above 120 eV can be assigned to f^0 final states.[26,25,24] In Fig. 11, the indicated splitting $\delta=3.4$ eV has almost the same value as the spin-orbit splitting of the La $4d$ states. The f^2 components located at the low-binding-energy side of the f^1 components in the Ce XPS spectrum (Fig. 10) are attributed within the Gunnarsson-Schönhammer model to the hybridization between the f states and the conduction band. The hybridization energy Δ, which describes the hybridization part of the Anderson impurity Hamiltonian, is defined as $\pi V^2 \rho_{\max}$, where $\rho_{\max}$ is the maximum in the density of the conduction states and V is the hybridization matrix element. Since the intensity ratio $r=I(f^2)/I(f^1)+I(f^2)$ for Ce has been calculated in Ref. 24 as a function of Δ, it is possible also to deduce the hybridization width Δ. The separation of the peaks in the Ce $3d$ XPS spectra (Fig. 10), which overlap, was made on the basis of the Doniach-Šunjić theory.[27] The ratio r could be determined with an accuracy of less than 5%. From the calculated variation of r as a function of Δ (Ref. 24), a hybridization width Δ of about 140 meV was obtained for CeRhSb and its alloys with an accuracy of 50 meV. For the doped samples, the hybridization constant slightly increases and changes the densities of states at the Fermi level (Table I). The change in hybridization is accompanied by the decrease in Kondo temperature. The r dependence on other parameters, such as the f-level occupancy, and the Coulomb interaction U between f electrons were not investigated. This analysis shows visible hybridization effects in the valence bands and good correlation with the susceptibility results.

Recently, we have discussed the mixed valence of Ce in CeNiSn and CeRhSb, which seems to be very important for the formation of the gap at the Fermi level.[28] It is a well-known fact that in every case there is an isostructural semiconductor in which Ce is replaced by a tetravalent non-$4f$ element, when the trivalent $4f$ analogs are metallic. In Ref. 28, we have argued for ZrNiSn and TiNiSn that the lowering

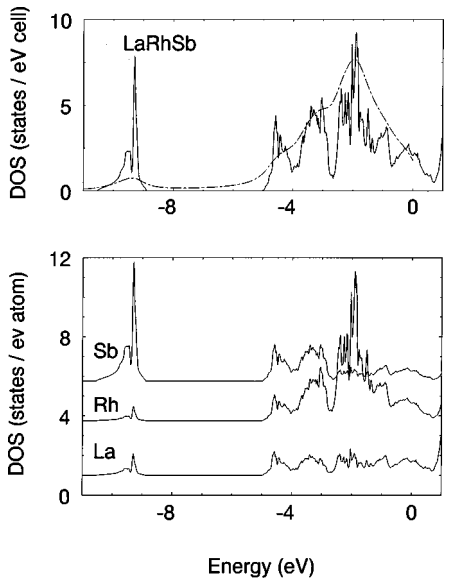

FIG. 12. Total DOS (solid line) and the convoluted DOS for LaRhSb. Partial DOS are shown below.

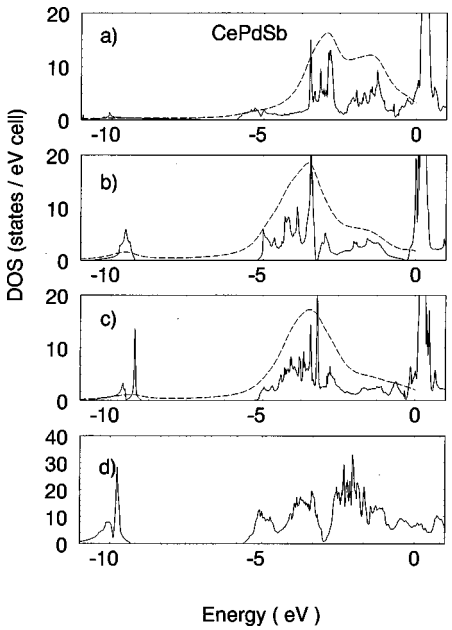

FIG. 13. The numerical calculations of DOS of CePdSb ($P6_3/mmc$) with different occupations of the crystallographic positions: (a) Ce atoms are in $2b$ $(6m2)$ sites and Pd and Sb accidentally are in $4f$ $(3m)$ sites, (b) Ce are in $2b$ and $4f$ sites are occupied by Pd, Sb, Pd, Sb . . . , (c) Ce are in $2b$ atomic positions and $4f$ sites. The total energy has the lowest value for the situation (b). In (d) the density of states is calculated for the frozen $4f$ states.

of the valence of Zr or Ti in the Ce-doped samples closes the gap at the Fermi level. A distinct correlation between the change of the gap at the *Y* point in Fig. 9 and the Ce valence in CeRhSb and in its doped samples gives the next evidence for that.

However, alloying also can affect the electronic structure in the vicinity of the gap, without a change in valence. Furthermore, the gap could be an intrinsic feature of the background band structure, e.g., of LaRhSb or CePdSb, so that the key role of the mixed valence would not be to create the gap, but to provide the extra electrons which move the Fermi level into the gap.

This is clearly visible in Figs. 12 and 13 with the numerical calculations of DOS. For LaRhSb, the pseudogap with the largest value at the *Y* point is located in the band at about 0.5 eV above ϵ_F. However, for trivalent CeRhSb this gap strongly depends on the crystallographic ordering and is located at about 0.5 eV below the Fermi level. Based on the numerical calculations, we show that for the mixed valence system the extra electron in the band can move the Fermi level exactly into the gap. In conclusion, we believe that both plausible effects can destroy the gap at the Fermi level as a consequence of the stable trivalence of Ce. In Fig. 13, we present the DOS calculations for the frozen $4f$ core states. The distribution of the densities of states without f-d hybridization is qualitatively the same as obtained for LaRhSb with nearly zero f occupation in La. We argue again that the f-d hybridization determines the formation of the gap at the Fermi level in ''Kondo-insulator''-type materials.

The following problem discussed here concerns the influence of the crystallographic ordering in the ''Kondo-insulator''-type materials on the gap. In Fig. 13, we present the results of numerical calculations for a different occupation of the atomic positions in CePdSb. The gap is evidently dependent on the local environment of the Ce atoms. It is also possible to obtain the gap with zero DOS very close to the Fermi level.

IV. CONCLUSIONS

CeRhSb is a strongly hybridized intermetallic compound with a hybridization energy of about 140 meV between f and the conduction states. The hybridization is also large when Rh or Sb are partly replaced by Pd, Co, or Sn. This hybridization leads to the formation of a narrow gap at the Fermi level in CeRhSb and similar Ce intermetallics. The present LMTO calculations of the electronic bands indicate, however, only a pseudogap with a very low DOS at ϵ_F. The energetic position of this pseudogap with respect to the Fermi level is shifted by alloying. We show that the shift depends on the change of the number of valence-band electrons in CeRhSb. Either increasing or decreasing this number, the DOS at ϵ_F always increases in the alloy with respect to CeRhSb. The $3d$ and $4d$ Ce XPS spectra clearly indicated the intermediate valence of Ce in CeRhSb and its Pd and Co alloys, in agreement with susceptibility measurements. The Sn alloy exhibits a valence close to 3, which is in disagreement with magnetic susceptibility measurements, which predict a valence of Ce larger than 3. LMTO calculations showed that the presence of Sn $5p$ states can completely remove the gap by hybridization. The mixed valence of Ce in these alloys is very important for the formation of the gap at ϵ_F. We discussed the changes in the partial DOS of Ce at ϵ_F for the Sn alloy due to the localization of the $5p$ states near the Fermi level, whereas for the remaining alloys the DOS is almost the same. The strong intra-atomic hybridization in the Sn alloy leads to an electronic band structure which is quite different from the one obtained for the Pd and Co alloys. The numerical calculations show that a V-shaped gap formation at the Fermi level is strongly dependent on the hybridization between the Ce $4f$ states and the transition-metal–d states. However, the local correlations have a destructive influence on the gap, and form the pseudogap with a small density of states at the Fermi level.

ACKNOWLEDGMENTS

This work was partly supported by the Foundation for Polish Science (Project SUBIN Nr 10/95), by the Deutscher Akademischer Austausch Dienst (DAAD), and by the Deutsche Forschungsgemeinschaft (DFG). One of us (A.J.) thanks the State Committee for Scientific Research for financial support (Project No. 2P03B118.14). The calculations were made in the Supercomputing and Networking Center of Poznań.

[1] T. Takabatake *et al.*, Jpn. J. Appl. Phys., Suppl. **26**, 547 (1987).
[2] T. Takabatake *et al.*, Phys. Rev. B **41**, 9607 (1990).
[3] S. K. Malik and D. T. Adroja, Phys. Rev. B **43**, 6277 (1991).
[4] M. F. Hundley *et al.*, Phys. Rev. B **42**, 6842 (1990).
[5] Z. Fisk *et al.*, Physica B **206&207**, 798 (1995).
[6] R. M. Martin, Phys. Rev. Lett. **48**, 362 (1982).
[7] F. G. Aliev *et al.*, Physica B **163**, 3581 (1990).
[8] T. Takabatake *et al.*, J. Magn. Magn. Mater. **76&77**, 87 (1988).
[9] P. Schlottmann, Phys. Rev. B **54**, 12 324 (1996).
[10] K. Nakamura *et al.*, Phys. Rev. B **53**, 6385 (1996); **54**, 6062 (1996).
[11] A. Ślebarski *et al.*, Phys. Rev. B **54**, 13 551 (1996).
[12] A. Ślebarski *et al.*, Phys. Rev. B **56**, 7245 (1997).
[13] Y. Baer, G. Busch, and P. Cohn, Rev. Sci. Instrum. **46**, 466 (1975).
[14] O. K. Andersen, O. Jepsen, and M. Sob, in *Electronic Structure and Its Applications*, edited by M. Yussouff (Springer, Berlin, 1987), p. 2.
[15] U. von Barth and L. Hedin, J. Phys. C **5**, 1629 (1972).
[16] C. D. Hu and D. C. Langreth, Phys. Scr. **32**, 391 (1985).
[17] A. Ślebarski, D. Wohlleben, and P. Weidner, Z. Phys. B **60**, 449 (1985).
[18] B. C. Sales and D. Wohlleben, Phys. Rev. Lett. **35**, 1240 (1975).
[19] J. Lawrence, Phys. Rev. B **20**, 3770 (1979).
[20] J. J. Yeh and I. Lindau, At. Data Nucl. Data Tables **32**, 1 (1985).
[21] S. Tougaard and P. Sigmund, Phys. Rev. B **25**, 4452 (1982).
[22] M. S. S. Brooks, L. Nordström, and B. Johansson, J. Phys.: Condens. Matter **3**, 2357 (1991).
[23] O. Gunnarsson and K. Schönhammer, Phys. Rev. B **28**, 4315 (1983).
[24] J. C. Fuggle *et al.*, Phys. Rev. B **27**, 7330 (1983).
[25] A. J. Signorelli and R. G. Hayes, Phys. Rev. B **8**, 81 (1973).
[26] Y. Baer *et al.*, Phys. Rev. B **18**, 4433 (1978).
[27] S. Doniach and M. Šunjić, J. Phys. C **3**, 286 (1970).
[28] A. Ślebarski *et al.*, Phys. Rev. B **57**, 9544 (1988).